Noname manuscript No.
(will be inserted by the editor)

Lens-shaped surfaces and C^2 subdivision

K. Karčiauskas · J. Peters

Received: date / Accepted: date

Abstract Lens-shaped surfaces (with vertices of valence 2) arise for example in automatic quad-remeshing. Applying standard Catmull-Clark subdivision rules to a vertex of valence 2, however, does not yield a C^1 surface in the limit. When correcting this flaw by adjusting the vertex rule, we discover a variant whose characteristic ring is $z \to z^2$. Since this conformal ring is of degree bi-2 rather than bi-3, it allows constructing a subdivision algorithm that works directly on the control net and generates C^2 limit surfaces of degree bi-4 for lens-shaped surfaces. To further improve shape, a number of re-meshing and re-construction options are discussed indicating that a careful approach pays off. Finally, we point out the analogy between characteristic configurations and the conformal maps $z^{4/n}$, $\cos z$ and e^z.

Keywords lens-shaped, C^2, subdivision surface, re-meshing, polar

Mathematics Subject Classification (2000) Computer aided design (modeling of curves and surfaces) · Splines · Computer graphics and computational geometry

1 Motivation

The prescription of the original Catmull-Clark construction [1] for creating a new mesh from an arbitrary existing one applies also when a vertex has valence $n = 2$ (Figure 2): For each facet, a new face node is computed as the average of the facet's old vertices; for each edge, a new edge node is introduced as the average of the edge's endpoints and the two new vertices of the faces joined by the edge; and for each vertex of valence n a new vertex node is computed as $(Q + 2R + (n-3)S)/n$

K. Karčiauskas
Vilnius University

J. Peters
University of Florida,
Tel.:(352)392-1226,
E-mail: jorg@cise.ufl.edu

where Q is the average of the new face nodes of all faces touching the old vertex S and R is the average of the midpoints of all old edges incident on S. A facet of the new mesh then consists in sequence of a vertex node, an edge node, a face node and a second edge node. However, applying these rules when $n = 2$ does not yield a C^1 limit surface, but results in section curves such as shown in Figure 1. Of course

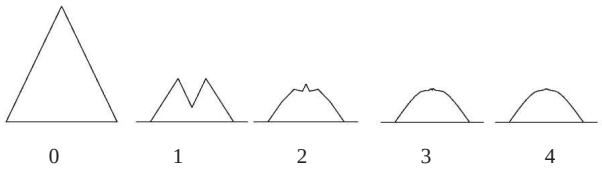

Fig. 1: Slice through **Catmull-Clark control net** after 0,1,2,3,4 applications of the rules for valence $n = 2$. The fluctuation is due to the -S/2 term corresponding to a subdominant eigenvalue $\lambda = -1/4$ (one of three eigenvalues of modulus $1/4$).

valence 2 can be avoided if the mesh is interactively designed (see Section 4) but lens-shaped surface blends do occur naturally as shown in Figure 16; and some recent remeshing techniques of scanned input into quad meshes [12, 3] inherently generate (pairs of) vertices of valence 2 such as in Figure 13. This, and the intellectual pursuit of covering all cases, no doubt motivated the earlier work on the subject [10, 7, 4].

This paper contributes the following insights into modeling lens-shaped surfaces completing a given surface.

- Section 2 explains how to change the Catmull-Clark rules to obtain a C^1 bi-3 subdivision for $n = 2$.
- Section 3 uses the characteristic ring of this approach to create a bi-4 subdivision algorithm that generates a C^2 lens-shape limit surface. While this result is remarkable for the theory of subdivision surfaces,
- better shape can be achieved by re-meshing the input in a non-trivial fashion (as explained in Section 4) or by re-constructing with polar layout according to Section 5.
- Section 6 discusses implications on the lower bound for C^2 subdivision and draws a parallel to elementary conformal maps.

2 C^1 Bicubic subdivision for $n = 2$

Except for the central point (and some interpretation of overlapping rules), our new subdivision rules in the vicinity of a vertex of valence $n = 2$ in the quad(rilateral) mesh (see Figure 3) will be identical to that of Catmull-Clark subdivision. Therefore, of the 25×25 subdivision matrix A, only the stencils that differ from the regular tensor-product refinement rules need to be shown in Figure 3.

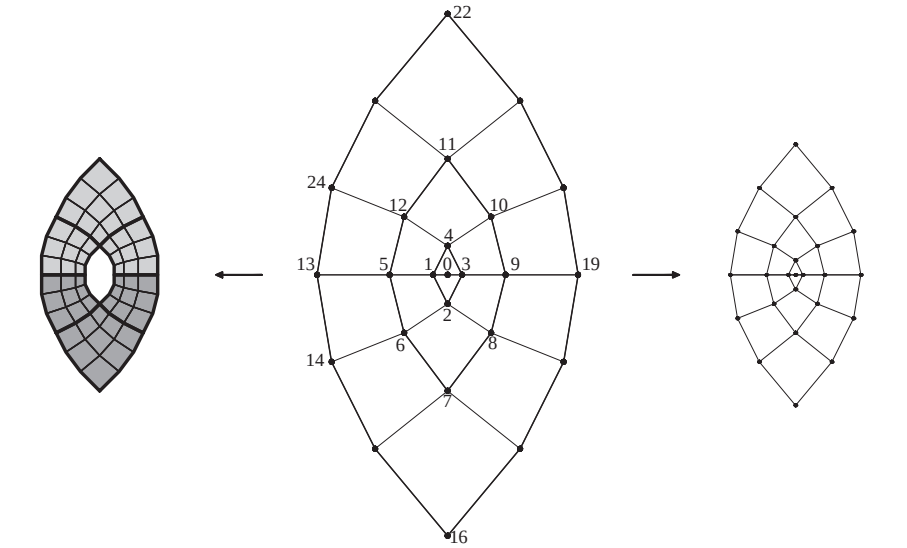

Fig. 2: **Bi-3 surface ring** (*left*) consisting of two L-shaped segments; (*middle*) counterclockwise indexing of mesh points $\mathbf{p}_i$, $i = 0, \ldots, 24$, for valence $n = 2$; (*right*) refined mesh.

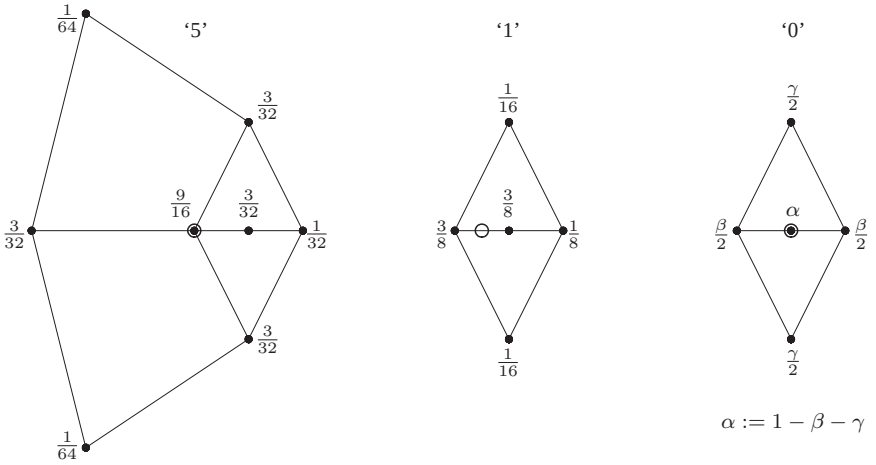

Fig. 3: **Stencils of bi-3** subdivision for $n = 2$. (From *left* to *right*) circled vertex labeled '5', '1' and '0'. Rules '5' and '1' are those of standard Catmull-Clark, taking overlap into account. The default choice for γ in '0' is $\gamma = 1/8$ so that we have a triple eigenvalue $1/8$; $\beta := 1/2$ sets an eigenvalue to zero.

The new rules generate a sequence of bicubic C^2 surface rings (see Figure 2) that is C^1 at the limit point. The characteristic polynomial of A is

$$\frac{h}{D}(\lambda-1)(4\lambda-1)^2(8\lambda-1)^2(16\lambda-1)^2(32\lambda-1)^2(64\lambda-1)^2\lambda^{12}, \qquad (1)$$
$$h := 16\lambda^2 + 4\lambda(4\beta+4\gamma-3) + 1 - 2\beta, \quad D := -17592186044416.$$

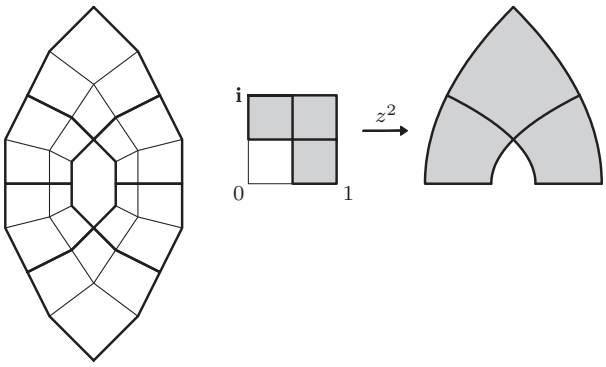

Fig. 4: The **characteristic ring** χ_2 **of bi-3** subdivision (*left*) is of degree bi-2 and (*right*) a sector is the conformal map $z \to z^2$.

For $\beta := 1/2$, $\gamma := 1/8$, we have $h = \lambda(16\lambda - 2)$ and we can read off the subdominant eigenvalue $1/4$ indicating rapid contraction.

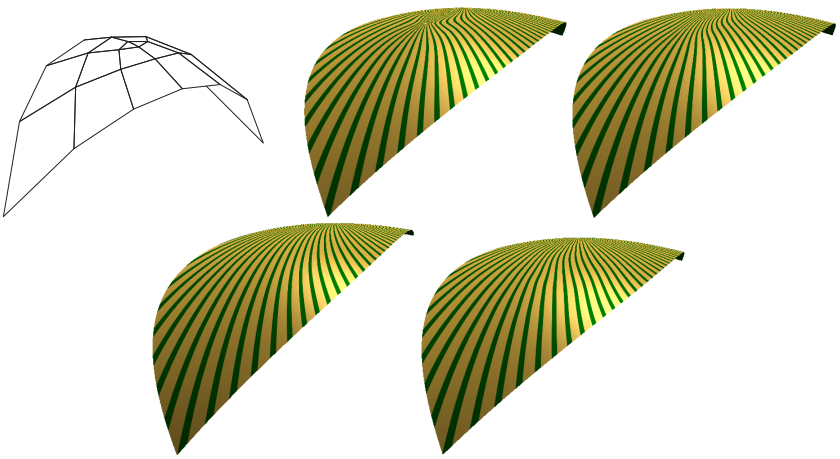

Fig. 5: **Comparison** by highlight lines. (*top left*) control net of χ_2 projected onto an elliptic paraboloid. (*top middle*) Bi-3 subdivision highlight lines indicate shape problems familiar from Catmull-Clark subdivision. (*top right*) The bi-4 subdivision surface of Section 3 is C^2 but the highlight line distribution is still unsatisfactory. (*bottom left*) Bi-4 subdivision after re-meshing according to Figure 10, (*bottom right*) re-meshing according to Figure 12.

The exciting observation is that the sub-eigenfunctions $\left[\begin{smallmatrix} f_1 \\ f_2 \end{smallmatrix}\right]$ are of degree bi-2. After enforcing rotational symmetry, we can set width and height so that a segment of the characteristic ring is defined by the spline coefficients (in the order of Figure 2 *middle*)

$$\frac{1}{4}\left[\begin{smallmatrix} 0 & 1 & 0 & -1 & 0 & 4 & 3 & 0 & -3 & -4 & -3 & 0 & 3 & 9 & 8 & 5 & 0 & -5 & -8 & -9 & -8 & -5 & 0 & 5 & 8 \\ 0 & 0 & 2 & 0 & -2 & 0 & 4 & 8 & 4 & 0 & -4 & -8 & -4 & 0 & 6 & 12 & 18 & 12 & 6 & 0 & -6 & -12 & -18 & -12 & -6 \end{smallmatrix}\right]$$

of the conformal map $z \to z^2$ (see Figure 4). Since the restriction of $z \to z^2$ is injective, the new bi-3 subdivision rules generate a surface that is C^1 at the extraordinary point. The left eigenvector of A corresponding to the eigenvalue 1 yields the extraordinary limit point

$$(1-\tilde{\beta}-\tilde{\gamma})\mathbf{p}_0 + \frac{\tilde{\beta}}{2}\Big(\mathbf{p}_1+\mathbf{p}_3\Big) + \frac{\tilde{\gamma}}{2}\Big(\mathbf{p}_2+\mathbf{p}_4\Big), \qquad (2)$$
$$\tilde{\beta} := \frac{12\beta+8\gamma}{14\beta+16\gamma+5}, \tilde{\gamma} := \frac{2\beta+8\gamma}{14\beta+16\gamma+5}.$$

An example is shown in Figure 5, *top middle*. Replacing the central point by an average of its neighbors $1, 2, 3, 4$, reduces any spikiness due to the small subdominant eigenvalue.

3 C^2 bi-4 subdivision

The C^2 bi-2 characteristic ring of the bi-3 subdivision presented in the previous section advertises itself as *concentric tessellation map* for guided subdivision [5]. Our construction and sampling of a guide surface of degree bi-5 to derive subdivision rules are sketched in Figures 8 and 9. The details are important to obtain good surface quality; but they are not needed for use of the algorithm since we can give *an explicit subdivision matrix* A, i.e. rules acting directly on the mesh.

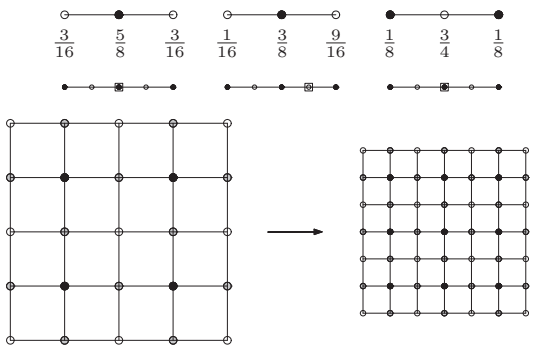

Fig. 6: **Regular Bi-4 subdivision** (*top*) univariate subdivision: 2-fold knots are displayed as black disks, 1-fold knots as circles; (*bottom*) tensored conversion. (black: 2,2 knot, gray: 2,1 knot, circle: 1,1 knot)

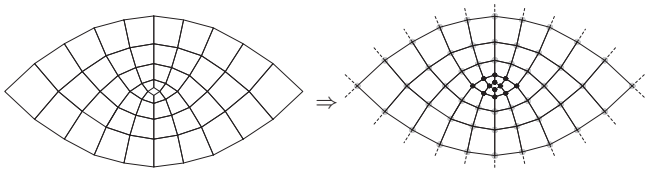

Fig. 7: C^2 **Bi-4 subdivision**. Note that the bi-4 lens mesh has no central point of valence 2. (*left*) mesh and (*right*) its scaled-up refinement. The gray points are defined by regular subdivision, the black ones by the rules (3).

By degree raising, we can switch from any bi-3 input to a bi-4 mesh with double knots. Figures 6 and 7 illustrate one step of bi-4 C^2 (double-knot) spline subdivision. As usual, repeated application yields a contracting sequence of surface rings. With the following rules, also the limit is an everywhere C^2 surface. The coefficients A_{ij}, $13 \leq i \leq 60$, $j = 1, \ldots, 60$ of the subdivision matrix A are defined by regular subdivision (see gray disks in Figure 7 *right*) and $A_{ij} = 0$ for $i = 1, \ldots, 12$; $j = 25, \ldots, 60$; so it suffices to define the stencils for coefficients 1–12 (indexing as in Figure 2, *middle*). Moreover, the coefficients A_{ij}, $j = 1 \ldots 24$, for $i = 3, 4, 8, 9, 10, 11, 12$ are recovered by symmetry from the scaled columns listed below: for $\kappa := 4194304$,

$$
\begin{array}{ccccc}
\kappa A_{1j}: & 8\kappa A_{2j}: & \kappa A_{5j}: & 16\kappa A_{6j}: & 8\kappa A_{7j}: \\
811090 & 5711612 & 1082610 & 13746012 & 3746052 \\
712980 & 7604042 & 655140 & 19897458 & 14524470 \\
651654 & 5711612 & 479430 & 7303932 & 3746052 \\
712980 & 4098598 & 655140 & 5091390 & 456666 \\
396360 & 2547228 & 578440 & 6720204 & 1288740 \\
192300 & 1874136 & 242700 & 6962248 & 4139016 \\
0 & -1392 & 0 & -17712 & 351344 \\
126420 & 1874136 & 45300 & 3288936 & 4139016 \\
271800 & 2547228 & 167544 & 2477004 & 1288740 \\
126420 & 793616 & 45300 & 297120 & -62832 \\
0 & 0 & 0 & 0 & 0 \\
192300 & 793616 & 242700 & 1342272 & -62832 \\
11070 & -12216 & 24030 & 110328 & -130440 \\
4155 & 53155 & 7995 & 334671 & 149757 \\
0 & 116 & 0 & -1404 & 14412 \\
0 & 0 & 0 & 0 & 0 \\
0 & 116 & 0 & 4356 & 14412 \\
-5535 & 53155 & -12015 & 975 & 149757 \\
-8310 & -12216 & -15990 & -258600 & -130440 \\
-5535 & -41055 & -12015 & -127179 & -33729 \\
0 & 0 & 0 & 0 & 0 \\
0 & 0 & 0 & 0 & 0 \\
0 & 0 & 0 & 0 & 0 \\
4155 & -41055 & 7995 & -63147 & -33729
\end{array}
\quad . \tag{3}
$$

For example, $A_{63} := \frac{7303932}{16\kappa}$. The subdivision matrix $A \in \mathbb{R}^{60\times 60}$ has the characteristic polynomial

$$
\begin{aligned}
&\frac{a_1 a_2 a_3 a_4}{D}(\lambda-1)(4\lambda-1)^2(16\lambda-1)^3(64\lambda-1)^3(256\lambda-1)^2\lambda^{36}, \\
a_1 :=& 134217728\lambda^2 - 2110592\lambda + 7487, \\
a_2 :=& 4503599617370496\lambda^3 - 75230110285824\lambda^2 \\
&+ 62486728704\lambda + 410899717, \\
a_3 :=& 2882303761517117744\lambda^4 - 7667169458388992\lambda^3 \\
&+ 19671721967616\lambda^2 + 397951106240\lambda - 1115103427, \\
a_4 :=& 2361183241434822606848\lambda^4 - 196790415217488035 84\lambda^3 \\
&+ 35225654240739328\lambda^2 + 91463875469312\lambda - 286255219911,
\end{aligned} \tag{4}
$$

where D is some 78-digits integer, all computed by Maple. The roots of the polynomials a_i are in modulus less than $1/16$. This eigenspectrum is consistent with the requirements of subdivision to be C^2 at the extraordinary point [8, Ch 7]. We verify that the characteristic ring (f_1, f_2), corresponding to subdominant eigenvalue $1/4$, agrees with that of the bi-3 subdivision of Section 2; and that the space spanned by

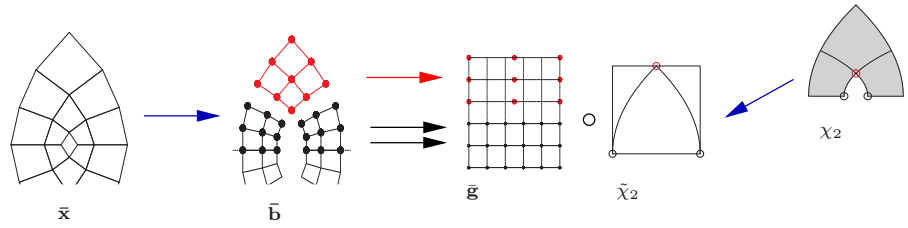

Fig. 8: **Construction of a guide surface g**. The guide surface consists of two C^2 connected patches each of degree bi-5, one per sector. We look at the top patch $\bar{\mathbf{g}}$. (*left*) The top segment $\bar{\mathbf{x}}$ of the bi-4 spline ring is converted to Bernstein-Bézier (BB) form and raised to degree bi-5 to yield the boundary data $\bar{\mathbf{b}}$. (*right*) The top sector of the characteristic ring χ_2 is translated and scaled so that the mid points and corner points of the resulting map $\tilde{\chi}_2$ fit tightly into the unit square domain of the bi-5 patch $\bar{\mathbf{g}}$. The guide patch $\bar{\mathbf{g}}$ is chosen so that its top rows are of degree 2 (raised to degree 5). — We now match the 3×3 jet of partial derivatives $(\partial_1^j \partial_2^k)_{0 \le j,k \le 2}$ of the composition $\bar{\mathbf{g}} \circ \tilde{\chi}_2$ to those of $\bar{\mathbf{b}}$. Such sampling at the *black circled* locations defines the bottom three rows of BB-coefficients (black points) of the guide patch. Sampling the jet at the *red circled* location yields the 3×3 derivatives that, due to the lowered degree, define the top three rows (red points) of $\bar{\mathbf{g}}$.

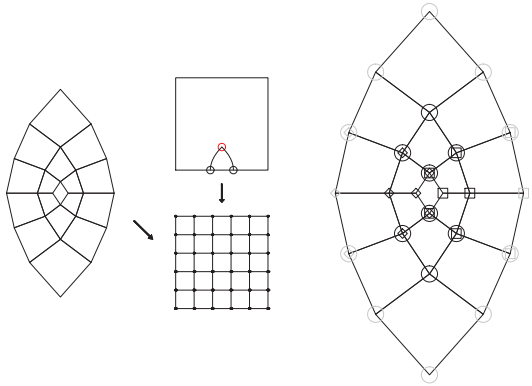

Fig. 9: **Sampling the guide surface** to derive A. The characteristic ring $\tilde{\chi}_2$ is scaled by its eigenvalue $1/4$ and the 3×3 jet of partial derivatives $(\partial_1^j \partial_2^k)_{0 \le j,k \le 2}$ of $\mathbf{g} \circ \frac{1}{4}\tilde{\chi}_2$ is sampled and converted into bi-4 double knot *spline* control points (*right*). The spline control points are averaged where overlapping. The square and diamond are the result of sampling at the locations marked (*middle top*) by the black circles, and those marked by a circle from a top or bottom (red circle) location.

the eigenfunctions corresponding to the subsubdominant eigenvalue $1/16$ is generated by f_1^2, $f_1 f_2$, f_2^2.

Figure 5,*top right* shows an example.

4 Remeshing

Although C^2, the bi-4 construction does not yield the shape quality one would hope for. This may be due to the two-sided overlap of the spline coefficients of one sector

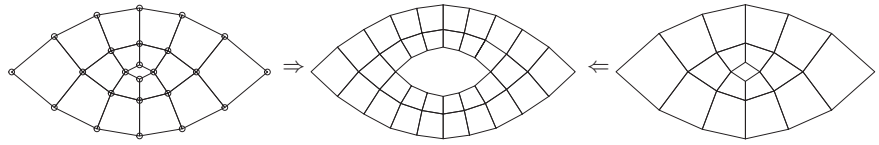

Fig. 10: **Re-meshing a bi-3 to a bi-4 mesh.** (*left*) The bi-3 mesh of Figure 2 (without central point) is degree-raised to four (with double knots) yielding the control net (*middle*); The bi-4 mesh (*right*) of Figure 7 (with the same combinatorial layout as *left*) is then determined so that, once subdivided, it best matches the *middle* mesh in the least squares sense; i.e., minimizes the sum of squared distances between corresponding control points.

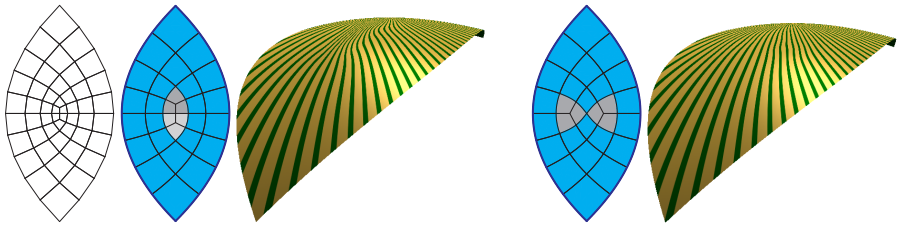

Fig. 11: Two **more re-meshing** strategies based on the setback strategy of Figure 10. The highlight lines of the strategy (*right*) are clearly more monotone.

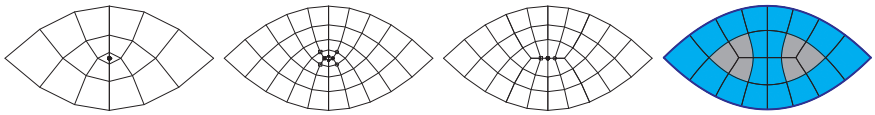

Fig. 12: **Re-meshing of a lens** by alternating subdivision and merging. (*left*) A bi-3 mesh with central vertex of valence 2. (*middle left*) Application of one bi-3 subdivision step as in Section 2. (*middle right*) The refined nodes, marked as quads, circles and disks, are averaged to new nodes. (*right*) The new mesh has separated 3-valent vertices but coincides with the original data and layout along the the lens's outer boundary. See Figure 14, *right*, for highlight lines on the surface.

with its neighbor (when $n > 2$, the left and right neighbor sector are distinct). In our experience, simple re-meshing does not solve the problem. Therefore in Figure 10 a more subtle remeshing is applied (whose effect is equivalent to degree elevation when the input is a characteristic control net). Refinement of the bi-4 mesh according to Section 3 then yields the black points of Figure 7; the grey points are defined by degree-elevating the input bi-3 mesh. The resulting bi-4 mesh defines one bi-4 ring that is C^2 connected to the surrounding outer ring and bi-4 subdivision can proceed. Figure 11 shows two more re-meshing strategies: (*left*) the central edges in Figure 10, *left*, are pairwise identified so that the valence 2 node disappears; (*right*) the central edges are removed. Then, in both cases one Catmull-Clark subdivision is applied. We observed that the *right* option results in visually significantly better surfaces. Another option, the re-meshing illustrated in Figure 12, results in fewer patches, typically of the same quality as the re-meshing of Figure 11, *right*. Both options should therefore be considered. For Figure 12, we create two valence-3 vertices. This and also the strategy in Figure 11, *right*, can be viewed as a local correction, via two 3-valent vertices, of automatic quad meshing algorithms generating lens-shapes [12].

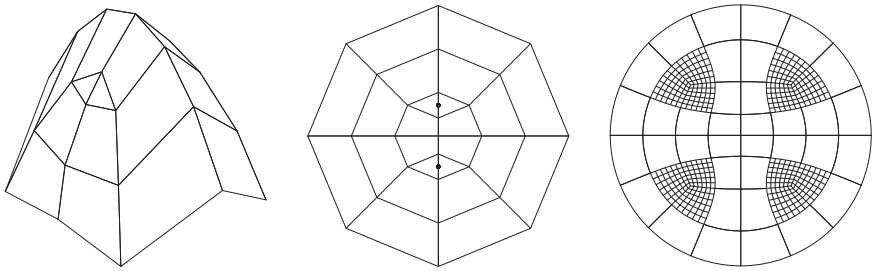

Fig. 13: **Paired lenses** (*left*) an elliptic paired lens mesh and the (*middle*) characteristic configuration of the paired lenses layout; (*right*) remeshed as in Figure 12 (with BB-coefficients of the fill displayed).

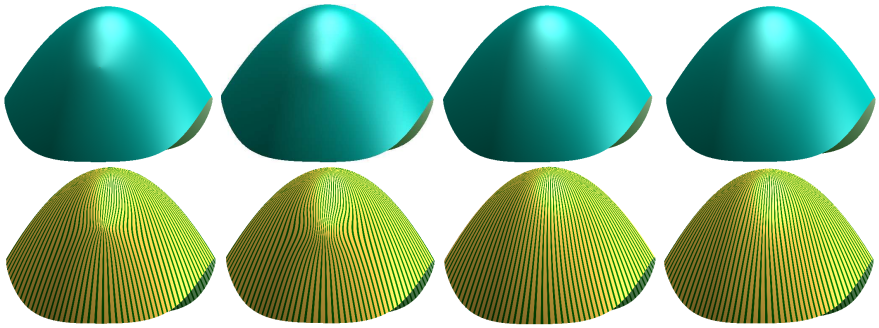

Fig. 14: **Paired lenses** example. (*left*) bi-3 subdivision; (*middle left*) bi-4 subdivision; (*middle right*) bi-4 subdivision after remeshing of Figure 10; (*right*) finite re-construction as in Figure 13.

In automatic reconstruction algorithms lenses occur in pairs such as in Figure 13, *left*, which illustrates the finger tips generated by [12]. Application of the re-meshing of Figure 12 yields the layout of Figure 13, *right*. Figure 14 compares this remeshing approach with bi-3 subdivision, bi-4 subdivision without remeshing and the polar re-construction explained next.

5 Polar re-construction

Polar mesh layout has one n-valent vertex surrounded by triangles, and such that the next layer is all quads and vertices of valence 4 [6]. But a number of *re-meshing* strategies for lens-shaped facets that we tried failed to deliver good surfaces. Indeed, the main challenge in constructing the lens-shaped surface with patches in polar layout is retaining good shape. The Appendix describes the details of a *polar re-construction* that results in good C^2 surfaces (based on guided surfacing). This polar patchwork consists of 16 patches, while the construction according to the layout of Figure 12 consists of 48 patches. Figure 16 shows a practical lens-shaped configuration that is best treated with polar re-construction. Another example (that should use polar layout or re-construction) are the finger tips of the hand shown shown in [3, Fig.10] and [2, Fig.20].

Characteristic configuration	layout	Conformal map
Section 2	valence $n = 2$	z^2
Section 4	pair $n = 2$	$\cos z$
Catmull-Clark	valence n	$z^{4/n}$
[6]	polar	e^z

Table 1: Correspondence of configurations and *conformal* neighborhoods.

Figure 17, *top left*, shows how the construction preserves and smoothly joins to the pre-existing boundary data.

6 Discussion

The construction of a bi-4 C^2 subdivision surface for $n = 2$ does not contradict the well-known lower bound estimate on the degree of subdivision surfaces [9]. That estimate asserts that an everywhere C^2 subdivision surfaces with 'L-shaped' segments must be at least of degree bi-6. However, the proof in [9] excludes the valences $n = 2, 4$. While the exclusion of $n = 4$ is obvious, the presented bi-4 C^2 subdivision shows that exclusion of $n = 2$ is not an artifact of the method of proof in [9] but is genuinely necessary.

It is unclear whether C^2 subdivision for $n = 2$ is helpful in creating high-quality surfaces without re-meshing: due the subdominant eigenvalue 1/4, the contraction is extremely fast and in our experiments, bi-4 subdivision without re-meshing did not fare as well as applying one step of the bi-3 subdivision followed by re-meshing.

We also want to share our observation that simple *re-meshing* of lens-pairs to polar layout resulted in surfaces clearly inferior to polar *re-constructed* surfaces with the help of a guide surface. Maybe, if polar structures would be considered in the original meshing of scanned data, the results could be better.

The discussion of lens-shaped regions and pairs of lens-shaped regions completes an interesting analogy between conformal maps and n-valent vertices in quad surface constructions ([8] credits D. Levin for pointing to the well-known map $z^{4/n}$ in the subdivision context. It is also mentioned in [13]). This correspondence in the layout of the parameter lines is illustrated in Figure 18 and tabulated in Table 1.

Acknowledgment:

Work supported in part by NSF Grant CCF-0728797.

References

1. E. Catmull and J. Clark, *Recursively generated B-spline surfaces on arbitrary topological meshes*, Computer Aided Design **10** (1978), 350–355.
2. Shen Dong, Scott Kircher, and Michael Garland, *Harmonic functions for quadrilateral remeshing of arbitrary manifolds*, Computer Aided Geometric Design **22** (2005), no. 5, 392–423.

3. Felix Kälberer, Matthias Nieser, and Konrad Polthier, *Quadcover - surface parameterization using branched coverings*, Comput. Graph. Forum **26** (2007), no. 3, 375–384.
4. K. Karciauskas, *Biangle surface patches*, Mathematical Methods for Curves and Surfaces Oslo 2000 (T. Lyche and L.L. Schumaker, eds.), Vanderbilt University Press, 2001, pp. 233–242.
5. K. Karčiauskas and J. Peters, *Concentric tesselation maps and curvature continuous guided surfaces*, Computer-Aided Geometric Design **24** (2007), no. 2, 99–111.
6. ———, *Surfaces with polar structure*, Computing **79** (2007), 309–315.
7. Kestutis Karciauskas and Rimvydas Krasauskas, *Rational biangle surface patches*, WSCG'98 Conference Proceedings (V. Skala, ed.), 1998.
8. J. Peters and U. Reif, *Subdivision surfaces*, Geometry and Computing, vol. 3, Springer-Verlag, New York, 2008.
9. U. Reif, *A degree estimate for subdivision surfaces of higher regularity*, Proc. Amer. Math. Soc. **124** (1996), no. 7, 2167–2174.
10. M. Sabin, *Two-sided patches suitable for inclusion in B-spline surfaces*, Mathematical Methods for Curves and Surfaces II (T. Lyche M. Dahlen and L.L. Schumaker, eds.), Vanderbilt University Press, 1998, pp. 409–416.
11. Boeing Corp. T. Grandine, *personal communication*, 2008.
12. Y. Tong, P. Alliez, D. Cohen-Steiner, and M. Desbrun, *Designing quadrangulations with discrete harmonic forms*, Eurographics Symposium on Geometry Processing (Cagliari, Sardinia, Italy) (Alla Sheffer and Konrad Polthier, eds.), Eurographics Association, 2006, pp. 201–210.
13. Denis Zorin and Peter Schröder, *A unified framework for primal/dual quadrilateral subdivision schemes*, Computer Aided Geometric Design **18** (2001), no. 5, 429–454.

Appendix: Polar construction details

In the polar (re-)construction, three circular B-spline layers surrounding the lens-shape (after removal of the central vertices of Figure 15 (a)) are raised to degree 5 in the radial direction Figure 19 (a). The outer, black points are known, the 3×8 gray points will be determined. Figure 19 (b) shows one patch in Bernstein-Bézier form corresponding to one sector of the C^2 polar ring (that extends the data in a C^2 fashion). Formal C^2 prolongation of the gray points towards the center and raising the circular direction to degree 6 results in n central patches of bidegree 6×5 such as the one shown in Figure 19 (c). The innermost layer of these 6×5 patches is collapsed to one point set to the location of the central point (red circle) of the bicubic patchwork in Figure 15 (b)). This leaves five of the six coefficients of the central quadratic expansion undetermined, in addition to the 3×8 (gray) spline coefficients. All 29 coefficients, for each coordinate separately, are determined by minimizing the two-norm of third derivatives of all patches.

Another alternative, shown to remove the need for one transition layer in Figure 17 *top*,*right*, increases the degree to bi-6 and has the inner coefficients, starting with the additional central circular layer, determined by minimizing the the two-norm of fourth derivatives of all patches.

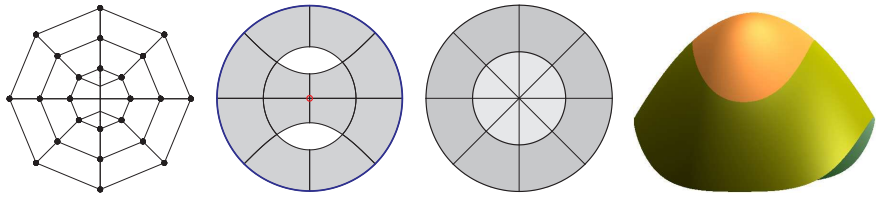

(a) (b) (c) (d)

Fig. 15: **Polar re-construction.** The construction via a guide surface based on the existing bi-3 mesh (a) The paired lenses configuration suggests polar layout. (b) Bi-3 patches (grey) with two lens-shaped holes yield a C^2 surface ring and the central point (red circle). (c) polar layout. (d) Resulting surface (either of degree 6,5 and C^2 or of degree 5,5 with no perceptible loss of quality, but formally not C^2.)

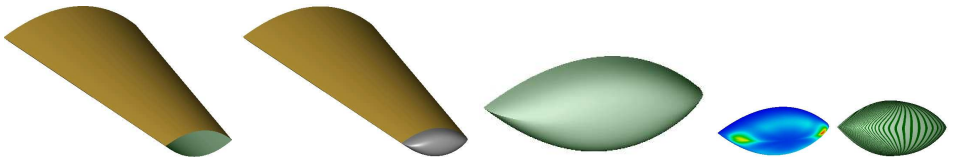

(a) input data (b) completed wing (c) cap of degree (6,5) (d) Gauss curvature and highlight lines

Fig. 16: **Wings** designed for supersonic and hypersonic speeds have sharp leading and sharp trailing edges [11].

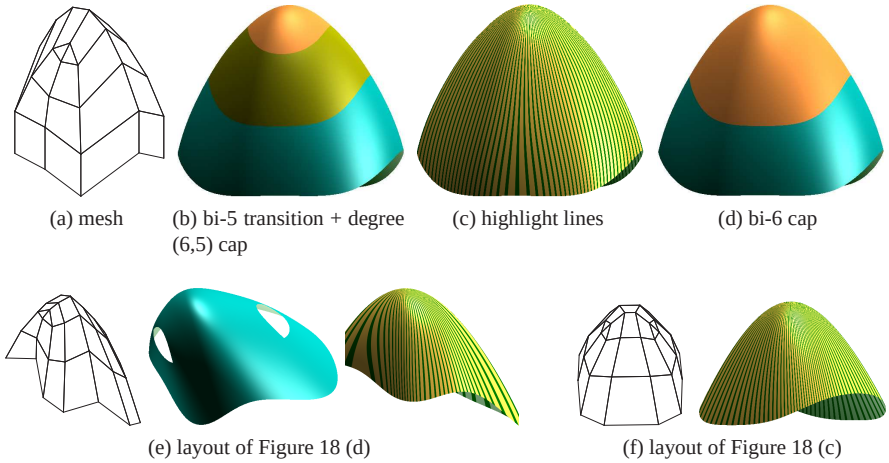

(a) mesh (b) bi-5 transition + degree (6,5) cap (c) highlight lines (d) bi-6 cap

(e) layout of Figure 18 (d) (f) layout of Figure 18 (c)

Fig. 17: **Polar re-construction** of paired lenses. (*top*) Surfaces from the mesh layout of Figure 18 (b) (extending the mesh of Figure 13 *left*). The input (outermost) ring is of degree bi-3. The caps have a collapsed edge (see Appendix). The highlight lines of both options are very similar. (*bottom*): Surfaces based on the layouts Figure 18 (c), (d).

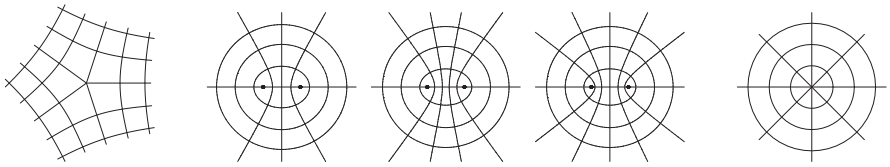

(a) $z^{4/n}$ (b) $\cos z$ (c) $\cos z$ (d) $\cos z$ (e) e^z

Fig. 18: Iso-parameter lines of **conformal** mappings corresponding to the characteristic maps of canonical subdivision strategies.

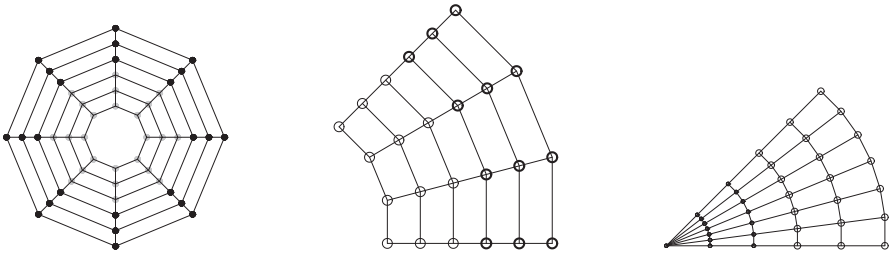

(a) B-spline layers (b) BB-net of a segment of the C^2 polar ring (c) BB-net of a segment of the C^2 central cap

Fig. 19: **Polar** construction of a transition and n central patches of degree 6,5.

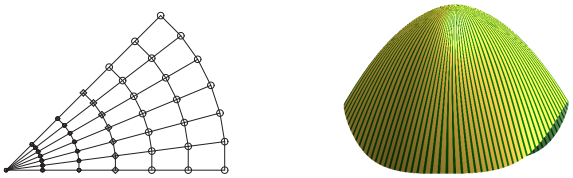

Fig. 20: Polar **bi-6 cap**.